Letter

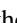# Determining the absolute number density of a thermal vapor via photon correlations

Sofia Ribeiro [1,2] Adrián Juan-Delgado [2] and Simon A. Gardiner [3]

[1]*Max Planck Institute for the Science of Light*, Staudtstraße 2, D-91058 Erlangen, Germany

[2]*Materials Physics Center*, CSIC-UPV/EHU, Paseo Manuel de Lardizabal 5, 20018 San Sebastián-Donostia, Basque Country, Spain

[3]*Joint Quantum Centre (JQC) Durham–Newcastle, Department of Physics, Durham University, South Road, Durham DH1 3LE, United Kingdom*

We propose a technique to determine the absolute number density N of an alkali-metal vapor confined within a nanocell. This method is based on near-resonant driving of the vapor's constituent atoms and determining the mean interparticle distance (or equivalently the temperature) from the power spectrum associated with the offset photon intensity-intensity correlation function $g^{(2)}(\tau) - 1$. In our investigation, we treat the atoms as an average of interacting and radiating dipole pairs randomly positioned within the nanocell. We observe that the power spectrum of the emitted light has a central dip for interparticle distances corresponding to $\sim \lambda/5$ and that this result is robust to variations in the driving Rabi frequency and the average detuning. With our proposed method, we can overcome the limitations in defining the absolute number density N, which is currently typically deduced from the temperature of heating elements applied externally to the cell.

Alkali-metal vapor cells have been used extensively in atomic physics since at least the 1950s [1–8]. Compared to laser-cooled and trapped atoms, experiments with thermal atomic vapors are simpler, cheaper, and more compact, while still offering high precision. Applications include atomic clocks [9,10], sensing [11–13], single-photon sources [14–16], other quantum technologies [17–20], and the study of fundamental physics [21–26]. Many exciting recent developments have been facilitated by spectroscopic micro- or nanocells. The key idea is to confine thermal atomic vapors, usually alkali-metal atoms (which, due to their simple electronic structure, are easier to model) in cells with the narrowest internal dimension as small as ~ 100 nm [27–32]. Typical cells are made of (transparent) dielectric materials such as sapphire, quartz, or fluoride [33,34]. One can vary the atomic number density over several orders of magnitude; high-density vapors allow interactions among atoms to be studied, for example, modifying light-matter interactions, leading to emission of quantum light from densely packed driven atoms [35–39].

To describe the physical processes occurring in such cells, or any physical quantities, it is typically necessary to know the atomic number density N. However, there is significant uncertainty in determining N in dense vapors, with its precise and accurate determination being a challenging task. If we have reliable vapor pressure curves, N can be inferred from the cell's temperature [40,41], assuming the atomic vapor is in thermal equilibrium with the condensed phase [42]. Due to its reactivity with the cell walls, this is often not true [43,44]. Moreover, there is always the issue of correctly measuring the temperature; there are, for example, deviations from the temperature applied externally to the cell compared to the temperature of the enclosed vapor. Recent work suggests a significantly more reliable thermometer based on Doppler-broadening thermometry [45], although to determine N we still depend on model-dependent vapor pressure curves [41].

It is also possible to determine N using absorption methods [46–48]. Although this does not assume thermal equilibrium, the determination of N depends on the product NL (where L is the path length through the vapor) and the oscillator strength f, as driven by the resonant light [42]. It is also only applicable for lower densities and not for optically thick vapors as the resonant light will be almost completely absorbed. For optically thick vapors, one can exploit the diamagnetic Faraday effect, as it is based on the far wing absorption line [42,49], or other methods, for example, using reduced absorption coefficients [50].

We propose a potentially more direct methodology to find N for hot, dense vapors confined within dielectric nanocells. We theoretically study the photon emission of an ensemble of interacting atoms, confined in a nanocell and driven by a coherent running laser field, as described in Ref. [51]. We closely model the experimental setup described in Refs. [29,52], where the photon statistics are measured via the total internal reflection fluorescence method [see Fig. 1(a)]. Although we focus on this configuration, the central point of this article is the photon number statistics, not the specific experimental setup. In this configuration, we study a form of power spectrum determined from $g^{(2)}(\tau) - 1$, where $g^{(2)}(\tau)$ is the intensity-intensity correlation function. For a thermal vapor, due to averaging over essentially random phase terms,
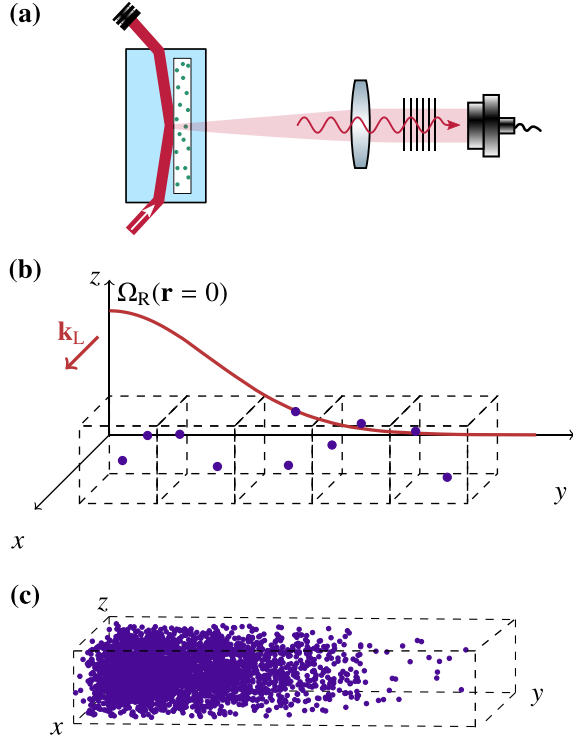
(a)

(b)

(c)

FIG. 1. Scheme of the geometry for the observation of intensity correlations. (a) Example of a measurement scheme of the photon statistics via the total internal reflection fluorescence method. A resonant laser beam enters a nanocell off axis, causing excitation and fluorescence in the atomic vapor. The photon statistics are considered to be measured at a point in the far-field zone of the radiation emitted by the atomic system. (b) In the theoretical model, we place pairs of atoms inside cubic boxes, the size of which ensures the desired average spacing, and place the different boxes in positions along the y direction according to a Gaussian distribution. (c) Example resulting from distribution of atomic pairs along the y axis, where the location of the pair determines the relevant value of Ω_R. The photon statistics are considered to be measured at a point in the far-field zone of the radiation emitted by the atomic system. For simplicity, we consider the direction of observation along the z axis, and the driving field $\mathbf{k}_L = (k_L, 0, 0)$. (Not to scale.)

our final result for the photon emission is independent of the observation angle, making our proposal insensitive to the light collection angle. For particular interatomic separations $\sim\lambda/5$, a characteristic central dip emerges in the power spectrum. Noting that, for a random three-dimensional (3D) distribution of atoms, the spacing between the atoms r has the distribution [53]

$$W_{3D}(r) = 4\pi N r^2 \exp\left(-\frac{4\pi}{3N r^3}\right), \qquad (1)$$

and the average distance between the atoms can be found from N to be

$$r_{av} = \int_0^\infty dr\, r W(r) \approx \frac{5}{9} N^{-1/3}. \qquad (2)$$

Hence, with this proposal we can systematically and independently measure the absolute number density N from photon correlations.

To describe the photon statistics of the nanocell confined thermal vapor, we use the same approach as in our previous article [51]. We consider two two-level atoms, at fixed positions $\mathbf{r}_1$ and $\mathbf{r}_2$ (where $\mathbf{r}_{12} = \mathbf{r}_1 - \mathbf{r}_2$), with the dipole moment $\mathbf{d}_{eg}$ for ground state $|g\rangle$ and excited state $|e\rangle$, and transition frequency ω_0. The atoms are driven by a running laser field with frequency ω_L. The system-reduced dipole density operator ρ evolves, in the laboratory frame, according to the master equation [39,54]

$$\frac{\partial\rho}{\partial t} = -i\omega_0 \sum_{j=1}^{2} [\hat{\sigma}_j^z, \rho] - \frac{i}{2} \sum_{j\neq l}^{2} g_{jl}[\hat{\sigma}_j^+\hat{\sigma}_l^- + \text{H.c.}, \rho]$$

$$+ \frac{i}{2} \sum_{j=1}^{2} [\Omega_j\hat{\sigma}_j^+ \exp(i\omega_L t) + \text{H.c.}, \rho]$$

$$- \sum_{j,l=1}^{2} \gamma_{jl}(\hat{\sigma}_j^+\hat{\sigma}_l^-\rho + \rho\hat{\sigma}_j^+\hat{\sigma}_l^- - 2\hat{\sigma}_l^-\rho\hat{\sigma}_j^+), \qquad (3)$$

where $\hat{\sigma}_j^+ = |e\rangle_{jj}\langle g|$ and $\hat{\sigma}_j^- = |g\rangle_{jj}\langle e|$ are the raising and lowering operators for the jth emitter, $\hat{\sigma}_j^z = (|e_i\rangle\langle e_i| - |g_i\rangle\langle g_i|)/2$, $2\gamma_{jj} = 2\Gamma$ is the Einstein A coefficient for spontaneous emission from a single dipole, and γ_{ij} ($i \neq j$) and g_{ij} are collective parameters describing the damping rate and the dipole-dipole coupling (the interatomic coupling arising from the mutual influence of the atoms through the electromagnetic field). We use the master equation (3) in the rotating-wave, Born, and Markoff approximations to produce coupled equations of motion for average values of the atomic operators and atomic correlations. We solve these coupled equations to find the dynamics for random pairs of emitters and average the photon statistics of multiple random pairs. In the limit of many atoms, the single-atom contributions to the photon statistics become unimportant relative to the two atoms' contributions and can safely be neglected (see Supplemental Material [55] and Ref. [51] for details).

In Refs. [56,57], the authors describe how a form of power spectrum, derived from $g^{(2)}(\tau) - 1$, can be used to gather information on the interatomic distance and orientation of two atoms. Our goal is to gather information on the *average* distance between atoms by modeling this power spectrum $S(\omega)$ when associated with light scattered by an atomic vapor. Following the same notation for coherence functions as in our previous work [51,58], we determine (and effectively define) $S(\omega)$ by taking the Fourier transformation of the autocorrelation function $g^{(2)}(\tau) - 1$:

$$S(\omega) = \int_{-\infty}^{+\infty} d\tau\, [g^{(2)}(\tau) - 1]e^{i(\omega-\omega_L)\tau}. \qquad (4)$$

Noting that generically $g^{(2)}(\tau) \to 1$ as $\tau \to \infty$, the -1 offset has the effect of ensuring the Fourier transform is always well-defined (removing a δ-peak contribution at $\omega = \omega_L$). As $g^{(2)}(\tau) = g^{(2)}(-\tau)$ and real, $S(\omega)$ is also necessarily real and symmetric about $\omega = \omega_L$ [59]. We consider a regime where antibunching may occur, meaning that the Siegert equation $g^{(2)}(\tau) - 1 = \beta|g^{(1)}(\tau)|^2$ does not apply; if $g^{(2)}(\tau) < 1$ (antibunched light), the left-hand side of the Siegert equation will be negative and therefore cannot equal the positively valued right [60]. From our previous studies [51], we have

shown that due to atom-atom interactions, our light source produces antibunched light at high temperatures. In particular, note that $S(\omega)$ is not the power spectrum associated with the fluorescence, but there is a nontrivial relation between the two. The experimental protocol is, therefore, to observe the photon statistics to determine $g^{(2)}(\tau)$ and then perform the Fourier transformation of the offset autocorrelation function $g^{(2)}(\tau) - 1$.

We perform a Monte Carlo simulation where pairs of atoms are placed randomly inside a cubic box, $(0, L) \times (-L/2, L/2) \times (-L/2, L/2)$, with the scale L chosen to ensure the desired average spacing (note there is a relationship between the size of the cubic box L and the average distance between two random points inside it, i.e., if $L = 1$, $\langle r_{ij} \rangle \approx 0.6617$). As in previous works [51,58], we set a minimum distance of 0.01λ between the two atoms; this codifies in a simple way that, at the energy scales under consideration, we do not expect the atomic dipoles to occupy the same space, which would in any case require inclusion of additional effects beyond the scope of the model. To account for Doppler broadening due to atomic motion, we assign a random velocity to each particle according to the Boltzmann distribution [61,62]. This is equivalent to randomly attributing a different detuning Δ_i to each atom around an average. For a thermal vapor, one would by default expect a broad atomic velocity distribution. However, we consider the vapor to be confined within a narrow nanocell. High-velocity atoms hit the cell walls and do not contribute to the measured photon statistics, i.e., only a narrow velocity window should be accounted for [29]. We therefore determine a temperature-dependent Gaussian distribution of detunings around a set average value, Δ_{av}, and truncate this to the restricted interval $\Delta_i = [\Delta_{\text{av}} - 5\,\Gamma, \ \Delta_{\text{av}} + 5\,\Gamma]$ (resulting in a nearly uniform distribution). Finally, to incorporate the "real" size of the cell, we average over the different boxes along the laser profile (see Fig. 1). To do so, we consider

$$\Omega_j = \Omega_{\text{R}} \exp(-i\,\mathbf{k}_{\text{L}} \cdot \mathbf{r}_j) \exp\left(-\frac{y_j}{2\sigma_{\text{L}}}\right), \qquad (5)$$

where we set $\mathbf{k}_{\text{L}} = (k_{\text{L}}, 0, 0)$. We average over spatially dependent Rabi frequencies by choosing randomly for each pair $y_i = y_{\text{box},i} + y_{\text{random}}$, where $y_{\text{box},i} \in [-L/2, \ L/2]$ and y_{random} is a random number following a Gaussian distribution with the standard deviation $\sigma_{\text{L}} = 3\lambda$. The final distribution of the 1500 pairs of emitters is depicted in Fig. 1(c). Such averaging, not considered in previous works [51,58], will not alter significantly the value of $g^{(2)}(0)$, but will reduce the oscillations of $g^{(2)}(\tau)$ over time, which is in accordance with experimental observations [52].

The approximate discrete equivalent of our continuous, infinite, power spectrum definition in Eq. (4), considering an interval of $\tau = -T$ to $\tau = T$, sampled at $2\mathcal{N}$ equally spaced points, is [63]

$$S(\ell/T) = \frac{2T\,\text{Re}(Q_\ell)}{\mathcal{N}P(\mathcal{N})}, \qquad (6)$$

where we have assumed a T value sufficiently large to set $g^{(2)}(-T) = g^{(2)}(T) = 1$, and where

$$Q_\ell = P(\mathcal{N}) \sum_{j=0}^{\mathcal{N}-1} [g^{(2)}(jT/\mathcal{N}) - 1]\, e^{2i\pi\ell j/\mathcal{N}} \qquad (7)$$

is the general form of an in-built numerical finite Fourier transformation (FFT), with $P(\mathcal{N})$ being an implementation-specific prefactor dependent on the number of sample points $\mathcal{N}$.

After finding numerical $g^{(2)}(\tau)$ for multiple pairs, we calculate $g^{(2)}(\tau) - 1$ in the interval $\tau\,\Gamma \in [0, 10]$ (i.e., $T = 10/\Gamma$) for $\mathcal{N} = 1000$ equally spaced values. The default numerical FFT implementation in MATHEMATICA we used to determine Q_ℓ has $P(\mathcal{N}) = \mathcal{N}^{-1/2}$, and we note that, although Eq. (6) shows that strict equivalence with the power spectrum of Eq. (4) requires taking the real part of Q_ℓ, in practice this makes little difference to the key features, and we find it sufficient to consider

$$|\mathcal{S}(\omega/\Gamma)| = \frac{2T\Gamma}{\sqrt{\mathcal{N}}} |Q_\ell|, \qquad (8)$$

where $\omega/\Gamma = 2\pi\ell/(T\,\Gamma)$. This is also consistent with the approach taken by Refs. [56,57] and is what we refer to as the power spectrum from now on.

For two two-level atoms, driven by a near-resonant standing laser field, the power spectrum exhibits several spectral lines, in frequency components related to the distance (dipole-dipole interaction strength) and position of the two atoms (Rabi frequency) [56,64]. In Ref. [57], when the dipole-dipole interaction is weak, the authors show the typical spectrum of two two-level atoms in a running laser field consists of five peaks; the middle peak occurs at ω_{L} and the two side peak doublets are symmetrically located at $\omega_{\text{L}} \pm \Omega_j(\mathbf{r}_j)$. Analyzing the power spectrum peaks gives us a direct measure of the position of each atom via the position-dependent Rabi frequencies. When the dipole-dipole interactions between the two atoms dominate the system dynamics, the side peaks move to the coupling strength energy $\omega_{\text{L}} \pm g_{12}$. In the intermediate regime, more peaks can be observed, with the splitting of the peak in $\omega_{\text{L}} \pm \Omega_j$ by the coupling strength, going from five to nine peaks. For both standing and running laser fields, this method also allows the determining of the orientation of two nearby atoms in arbitrary geometry, where the peak structure can be interpreted in terms of the system's dressed states [56,57,64].

In Fig. 2, we depict calculated spectra emitted from a many-atom system driven by a resonant laser field ($\omega_{\text{L}} = \omega_0$). We perform our simulation for multiple atomic pairs in a running-wave laser field with $\Omega_{\text{R}}(r = 0) = 20\,\Gamma$, where we fix the average values of detuning for both atoms at $\Delta_{\text{av}}/\Gamma = 0$, for different atomic distances. We compare these results to an idealized system of pairs at a fixed distance and a random distribution in space, shown as the dash-dotted lines. For each data point, we run the simulation over 1500 pairs. We observe three defined broad peaks; a central peak at $\omega - \omega_{\text{L}} = 0$ and two side peaks at $\omega - \omega_{\text{L}} = \pm\Omega_{\text{R}}(r = 0) = \pm 20\,\Gamma$. At such small atom-atom distances, $\Omega_1 \approx \Omega_2$, and the doublet peaks observed at $\omega_{\text{L}} \pm \Omega_j$ for two two-level atoms become single broader peaks. Moreover, in Fig. 2, as we approach
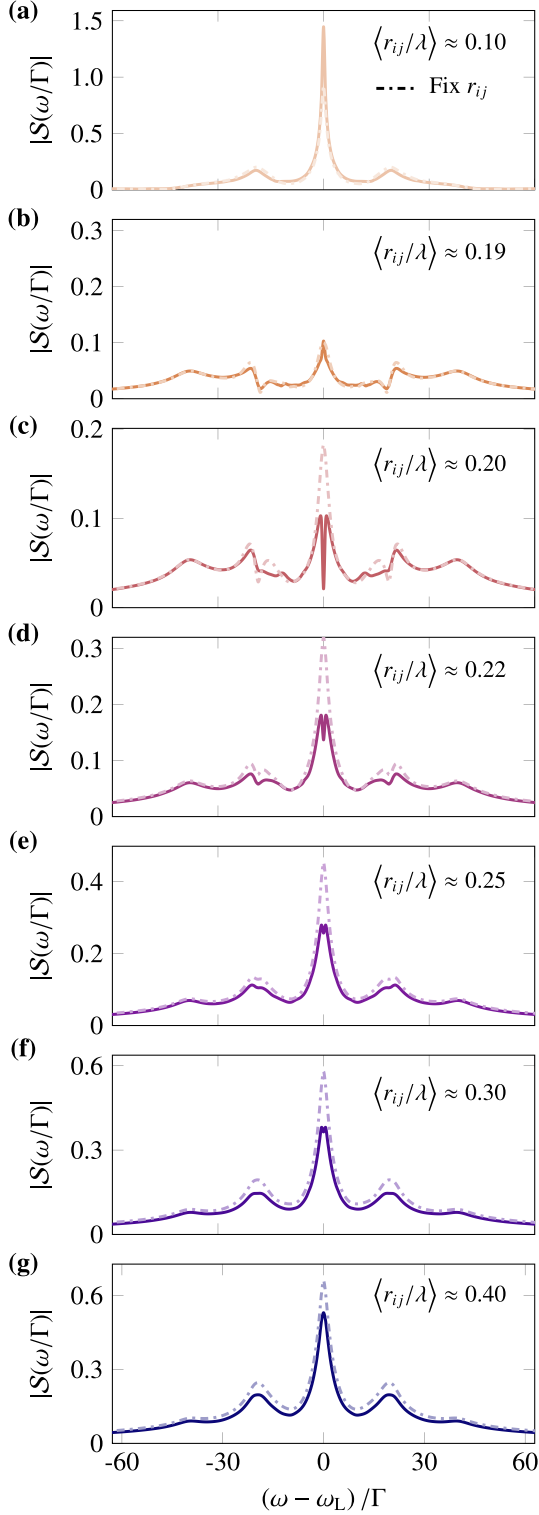
FIG. 2. Power spectrum peaks for multiple atomic pairs in a running-wave laser field with $\Omega_R(r=0)/\Gamma = 20$, where we have fixed the average values of detuning for both atoms at Δ_{av}/Γ equal to 0. We plot $|\mathcal{S}(\omega/\Gamma)|$ [defined in Eq. (8)] as a function of angular frequency for different atomic distances $0.10 \leqslant \langle r_{ij}/\lambda \rangle \leqslant 0.40$, and we compare the results with a configuration where the two atoms are at a fixed distance (dash-dotted line). For each data point, we run the simulation over 1500 pairs. Units are chosen such that the quantities are scaled by λ or Γ.
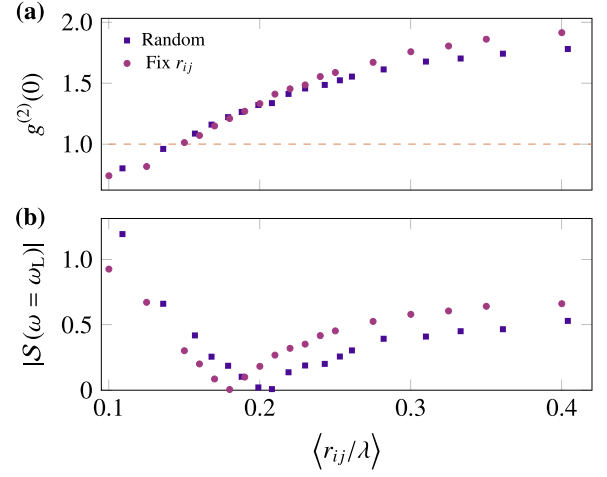

FIG. 3. (a) $g^{(2)}(0)$ (see also Refs. [51,58]) and (b) $|\mathcal{S}(\omega = \omega_L)|$ [see Eq. (8)] as functions of different atomic distances $\langle r_{ij}/\lambda \rangle$. We compare the case of randomly positioned pairs (squares) separated on average by $\langle r_{ij}/\lambda \rangle$ with the two atoms a fixed distance apart (circles). The atomic pairs are subjected to a running-wave laser field with $\Omega_R(r=0)/\Gamma = 20$, where we have fixed the average values of detuning for both atoms at Δ_{av}/Γ equal to 0. For each data point, we run the simulation over 1500 pairs. Units are chosen such that the quantities are scaled by λ or Γ.

$\langle r_{ij} \rangle \to \lambda/5$, we observe splitting of the peak at $\omega - \omega_L = \pm \Omega_R(r=0) = \pm 20\,\Gamma$ (clearer in the dashed lines, where the atoms are at idealized fixed distances) and also of the central line, which at $\omega - \omega_L = 0$ of the spectrum can go to 0.
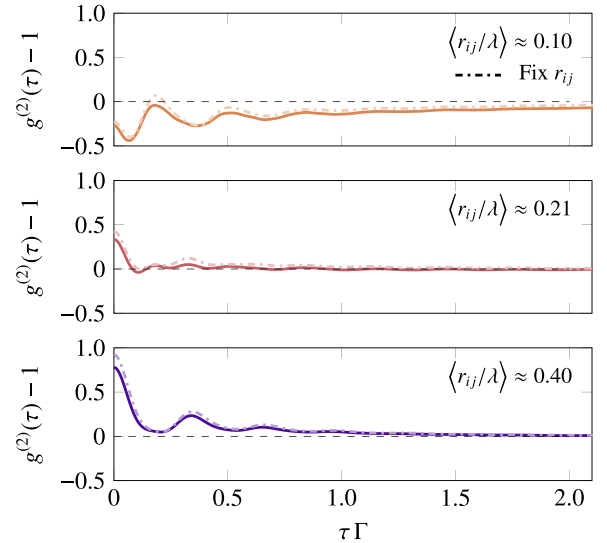

FIG. 4. $g^{(2)}(\tau) - 1$ (see also Refs. [51,58]) for multiple atomic pairs in a running-wave laser field with $\Omega_R(r=0)/\Gamma = 20$, where we have fixed the average values of detuning for both atoms at Δ_{av}/Γ equal to 0. We plot $g^{(2)}(\tau) - 1$ as a function of delay time for different atomic distances $\langle r_{ij}/\lambda \rangle \approx 0.10, 0.21$, and 0.40, and we compare the results with a configuration where the two atoms are at a fixed distance (dash-dotted line). For each data point, we run the simulation over 1500 pairs. Units are chosen such that the quantities are scaled by λ or Γ.

In Fig. 3, we consider how the values for (a) $g^{(2)}(\tau = 0)$ and (b) $|\mathcal{S}(\omega - \omega_L = 0)|$ vary with average atomic distance $\langle r_{ij}/\lambda \rangle$. The emergence of a spectral dip is due to the competition of different physical effects: the intensity of driving, and the dipole-dipole coupling strength. The change of behavior from bunching to antibunching can be correlated to the appearance of the dip, due to a distance-dependent crossover in the averaging of the pairs. In fact, $\mathcal{S}(\omega - \omega_L = 0) \to 0$; i.e., a dip emerges whenever we find $\int d\tau \, [g^{(2)}(\tau) - 1] \to 0$ [setting $\omega = \omega_L$ in Eq. (4)]. In this distance regime, $g^{(2)}(\tau)$ remains relatively close to 1 with small deviations, hence $g^{(2)}(\tau) - 1$ (averaged over different pairs) tends at a faster rate to 0 as $\tau \to \infty$, i.e., pairs of emitted photons are uncorrelated after shorter delay times (see Fig. 4). When we look at the region $0.19 \leqslant \langle r_{ij}/\lambda \rangle \leqslant 0.25$ (see Fig. 2), a small dip can still be observed for fixed distances at $\langle r_{ij}/\lambda \rangle = 0.18$, although the contrast could be challenging to resolve experimentally. This effect is nonetheless clear looking just at the values of $|\mathcal{S}(\omega - \omega_L = 0)|$ in Fig. 3. Were we to consider the real rather than the absolute values of $\mathcal{S}(\omega)$, we would see a crossover between positive and negative values when $\langle r_{ij} \rangle \sim \lambda/5$. This is robust to changes in detuning or driving (see Ref. [55]).

In conclusion, we have presented a proposal for determining the absolute number density N in a hot alkali-metal vapor confined within a nanocell. Our theoretical investigations show that, by studying the emergence of a dip in the power spectrum $\mathcal{S}(\omega)$, it is possible to infer the average atomic distance in the vapor cell. Since average atomic distance, temperature, and density are straightforwardly interrelated, we can then determine the number density, which in turn could be fed into, e.g., next-generation thermometry protocols based on Doppler broadening.

We repeat that this is not the power spectrum directly connected to fluorescence and that the protocol in a real experiment is to measure the intensity-intensity correlation function $g^{(2)}(\tau)$ of the emitted light field for different applied temperatures and to evaluate $\mathcal{S}(\omega)$ from it, by taking the Fourier transform of $g^{(2)}(\tau) - 1$. From this, we can extract spatial information and the corresponding absolute number density. This method provides a straightforward, precise approach to determine the absolute number density.

[1] B. Ai, D. S. Glassner, R. J. Knize, and J. P. Partanen, Appl. Phys. Lett. **64**, 951 (1994).

[2] S. Briaudeau, D. Bloch, and M. Ducloy, Europhysics Lett. **35**, 337 (1996).

[3] B. Zambon and G. Nienhuis, Opt. Commun. **143**, 308 (1997).

[4] S. Briaudeau, S. Saltiel, G. Nienhuis, D. Bloch, and M. Ducloy, Phys. Rev. A **57**, R3169(R) (1998).

[5] D. Sarkisyan, D. Bloch, A. Papoyan, and M. Ducloy, Opt. Commun. **200**, 201 (2001).

[6] G. Dutier, A. Yarovitski, S. Saltiel, A. Papoyan, D. Sarkisyan, D. Bloch, and M. Ducloy, Europhys. Lett. **63**, 35 (2003).

[7] J. E. Sharping, Nat. Photonics **1**, 315 (2007).

[8] T. Baluktsian, C. Urban, T. Bublat, H. Giessen, R. Löw, and T. Pfau, Opt. Lett. **35**, 1950 (2010).

[9] L.-A. Liew, S. Knappe, J. Moreland, H. Robinson, L. Hollberg, and J. Kitching, Appl. Phys. Lett. **84**, 2694 (2004).

[10] J. Vanier, Appl. Phys. B **81**, 421 (2005).

[11] J. R. Maze, P. L. Stanwix, J. S. Hodges, S. Hong, J. M. Taylor, P. Cappellaro, L. Jiang, M. V. G. Dutt, E. Togan, A. S. Zibrov, A. Yacoby, R. L. Walsworth, and M. D. Lukin, Nature (London) **455**, 644 (2008).

[12] J. Kitching, S. Knappe, and E. A. Donley, IEEE Sens. J. **11**, 1749 (2011).

[13] E. Klinger, H. Azizbekyan, A. Sargsyan, C. Leroy, D. Sarkisyan, and A. Papoyan, Appl. Opt. **59**, 2231 (2020).

[14] B. Lounis and M. Orrit, Rep. Prog. Phys. **68**, 1129 (2005).

[15] A. Dussaux, T. Passerat de Silans, W. Guerin, O. Alibart, S. Tanzilli, F. Vakili, and R. Kaiser, Phys. Rev. A **93**, 043826 (2016).

[16] F. Ripka, H. Kübler, R. Löw, and T. Pfau, Science **362**, 446 (2018).

[17] P. D. D. Schwindt, S. Knappe, V. Shah, L. Hollberg, J. Kitching, L.-A. Liew, and J. Moreland, Appl. Phys. Lett. **85**, 6409 (2004).

[18] H. J. Kimble, Nature (London) **453**, 1023 (2008).

[19] A. I. Lvovsky, B. C. Sanders, and W. Tittel, Nat. Photonics **3**, 706 (2009).

[20] T. H. Sander, J. Preusser, R. Mhaskar, J. Kitching, L. Trahms, and S. Knappe, Biomed. Opt. Express **3**, 981 (2012).

[21] J. Marek, J. Phys. B: At. Mol. Opt. **12**, L229 (1979).

[22] C. I. Sukenik, M. G. Boshier, D. Cho, V. Sandoghdar, and E. A. Hinds, Phys. Rev. Lett. **70**, 560 (1993).

[23] J. Keaveney, A. Sargsyan, U. Krohn, I. G. Hughes, D. Sarkisyan, and C. S. Adams, Phys. Rev. Lett. **108**, 173601 (2012).

[24] J. Petersen, J. Volz, and A. Rauschenbeutel, Science **346**, 67 (2014).

[25] P. Lodahl, S. Mahmoodian, S. Stobbe, A. Rauschenbeutel, P. Schneeweiss, J. Volz, H. Pichler, and P. Zoller, Nature (London) **541**, 473 (2017).

[26] T. Peyrot, Y. R. P. Sortais, A. Browaeys, A. Sargsyan, D. Sarkisyan, J. Keaveney, I. G. Hughes, and C. S. Adams, Phys. Rev. Lett. **120**, 243401 (2018).

[27] H. Kübler, J. P. Shaffer, T. Baluktsian, R. Löw, and T. Pfau, Nat. Photonics **4**, 112 (2010).

[28] K. A. Whittaker, J. Keaveney, I. G. Hughes, A. Sargsyan, D. Sarkisyan, B. Gmeiner, V. Sandoghdar, and C. S. Adams, J. Phys.: Conf. Ser. **635**, 122006 (2015).

[29] T. Cutler, W. Hamlyn, J. Renger, K. Whittaker, D. Pizzey, I. Hughes, V. Sandoghdar, and C. Adams, Phys. Rev. Appl. **14**, 034054 (2020).

[30] D. Pizzey, J. D. Briscoe, F. D. Logue, F. S. Ponciano-Ojeda, S. A. Wrathmall, and I. G. Hughes, New J. Phys. **24**, 125001 (2022).

[31] G. Ferioli, S. Pancaldi, A. Glicenstein, D. Clément, A. Browaeys, and I. Ferrier-Barbut, Phys. Rev. Lett. **132**, 133601 (2024).

[32] L. Donati, F. S. Cataliotti, and S. Gherardini, arXiv:2402.16056.

[33] S. Knappe, V. Velichansky, H. G. Robinson, J. Kitching, and L. Hollberg, Rev. Sci. Instrum. **74**, 3142 (2003).

[34] J. Kitching, Appl. Phys. Rev. **5**, 031302 (2018).

[35] H. S. Freedhoff, Phys. Rev. A **19**, 1132 (1979).

[36] T. Richter, Opt. Acta **29**, 265 (1982).

[37] R. D. Griffin and S. M. Harris, Phys. Rev. A **25**, 1528 (1982).

[38] Z. Ficek, R. Tanaś, and S. Kielich, Phys. Rev. A **29**, 2004 (1984).

[39] T. G. Rudolph, Z. Ficek, and B. J. Dalton, Phys. Rev. A **52**, 636 (1995).

[40] A. N. Nesmeyanov, *Vapor Pressure of Chemical Elements* (Izd. Akad. Nauk SSSR, Moscow, 1961).

[41] C. B. Alcock, V. P. Itkin, and M. K. Horrigan, Can. Metall. Q. **23**, 309 (1984).

[42] Z. Wu, M. Kitano, W. Happer, M. Hou, and J. Daniels, Appl. Opt. **25**, 4483 (1986).

[43] M. A. Bouchiat and J. Brossel, Phys. Rev. **147**, 41 (1966).

[44] X. Zeng, Z. Wu, T. Call, E. Miron, D. Schreiber, and W. Happer, Phys. Rev. A **31**, 260 (1985).

[45] N. Agnew, G. Machin, E. Riis, and A. S. Arnold, arXiv:2307.06229.

[46] B. Shirinzadeh and C. C. Wang, Appl. Opt. **22**, 3265 (1983).

[47] V. Horvatic, M. Movre, R. Beuc, and C. Vadla, J. Phys. B: At. Mol. Opt. **26**, 3679 (1993).

[48] C. Vadla, V. Horvatic, and K. Niemax, Appl. Phys. B **84**, 523 (2006).

[49] S. L. Kemp, I. G. Hughes, and S. L. Cornish, J. Phys. B: At., Mol. Opt. Phys. **44**, 235004 (2011).

[50] V. Horvatic, D. Veza, K. Niemax, and C. Vadla, Spectrochim. Acta B **63**, 210 (2008).

[51] S. Ribeiro, T. F. Cutler, C. S. Adams, and S. A. Gardiner, Phys. Rev. A **104**, 013719 (2021).

[52] W. J. Hamlyn, Ph.D. thesis, Durham University, 2020.

[53] S. Chandrasekhar, Rev. Mod. Phys. **15**, 1 (1943).

[54] Z. Ficek and R. Tanaś, Phys. Rep. **372**, 369 (2002).

[55] See Supplemental Material at http://link.aps.org/supplemental/10.1103/PhysRevA.110.L031701 for more details on the calculations.

[56] J.-T. Chang, J. Evers, and M. S. Zubairy, Phys. Rev. A **74**, 043820 (2006).

[57] Qurrat-ul-Ain Gulfam and J. Evers, J. Phys. B: At., Mol. Opt. Phys. **43**, 045501 (2010).

[58] S. Ribeiro and S. A. Gardiner, Phys. Rev. A **105**, L021701 (2022).

[59] We follow the convention in presenting $S(\omega)$ as a function of ω; however, note that, as a Fourier transform of $g^{(2)}(\tau) - 1$, the conjugate variable is in fact $\omega - \omega_L$.

[60] For a thermal or chaotic light source, the Siegert equation $g^{(2)}(\tau) - 1 = \beta |g^{(1)}(\tau)|^2$ holds, where β depends on the spatial coherence of the light detection system [66], and the fluorescence spectrum [i.e., the Fourier transform of $g^{(1)}(\tau)$] can be determined from $g^{(2)}(\tau)$.

[61] J. Javanainen, J. Ruostekoski, Y. Li, and S.-M. Yoo, Phys. Rev. Lett. **112**, 113603 (2014).

[62] J. Javanainen, J. Ruostekoski, Y. Li, and S.-M. Yoo, Phys. Rev. A **96**, 033835 (2017).

[63] The literal discrete approximant to our continuous, infinite, definition of power spectrum in Eq. (4) is $S(k\Delta\nu) = (T/\mathcal{N})\sum_{j=-\mathcal{N}}^{\mathcal{N}-1}[g^{(2)}(j\Delta\tau) - 1]e^{i\pi jk/\mathcal{N}}$, where $\Delta\tau = T/\mathcal{N}$, $\Delta\nu = 1/(2T)$, and $\nu = (\omega - \omega_L)/(2\pi)$. As both $g^{(2)}(j\Delta\tau)$ and $S(k\Delta\nu)$ are real and symmetric, $S(\ell/T) = 2T\,\mathrm{Re}(Q_\ell)/[\mathcal{N}P(\mathcal{N})] - T[g^{(2)}(0) - 1]/\mathcal{N}$, where Q_ℓ is defined in Eq. (7), and we assume $g^{(2)}(-T) = g^{(2)}(T) = 1$. For any reasonably large $\mathcal{N}$, the second term of $S(\ell/T)$ can typically be considered inconsequential and therefore neglected, leading to Eq. (6).

[64] J.-T. Chang, J. Evers, M. O. Scully, and M. Suhail Zubairy, Phys. Rev. A **73**, 031803(R) (2006).

[65] S. Ribeiro, Dataset for "Determining the absolute number density of a thermal vapor via photon correlations", doi:10.17617/3.IZM9HA (2024).

[66] K. Muhammed Shafi, D. Pandey, B. Suryabrahmam, B. S. Girish, and H. Ramachandran, J. Phys. B: At., Mol. Opt. Phys. **49**, 025301 (2016).